Potential impact of photoinhibition on microphytobenthic primary production on a large intertidal mudflat

R. Savelli, J. Serôdio, P. Cugier, V. Méléder, P. Polsenaere, C. Dupuy, Vincent Le Fouest

JGR Biogeosciences

RESEARCH ARTICLE
10.1029/2021JG006443

Potential Impact of Photoinhibition on Microphytobenthic Primary Production on a Large Intertidal Mudflat

Raphaël Savelli[1], João Serôdio[2], Philippe Cugier[3], Vona Méléder[4], Pierre Polsenaere[5], Christine Dupuy[1], and Vincent Le Fouest[1]

[1]LIttoral, ENvironnement et Sociétés (LIENSs), Université de La Rochelle, CNRS-ULR, La Rochelle, France, [2]CESAM—Universidade de Aveiro, Campus Universitário de Santiago, Aveiro, Portugal, [3]Département Dynamiques de l'Environnement Côtier, Laboratoire d'Ecologie Benthique, Plouzané, France, [4]Université de Nantes, Mer Molécules Santé, Nantes Cedex, France, [5]IFREMER, Laboratoire Environnement Ressources des Pertuis Charentais (LER/PC), La Tremblade, France

Key Points:

- With or without photoinhibition, simulated yearly MPB PP is higher on the upper and middle shores than on the lower shore
- Photoinhibition leads to a 20% (-0.79×10^3 t C yr^{-1}) decrease of MPB PP over the entire mudflat
- The photoinhibition process in the model is sensitive to the photoacclimation status of MPB cells

Correspondence to:
R. Savelli,
raphael.savelli1@univ-lr.fr

Citation:
Savelli, R., Serôdio, J., Cugier, P., Méléder, V., Polsenaere, P., Dupuy, C., & Le Fouest, V. (2021). Potential impact of photoinhibition on microphytobenthic primary production on a large intertidal mudflat. *Journal of Geophysical Research: Biogeosciences*, *126*, e2021JG006443. https://doi.org/10.1029/2021JG006443

Received 6 JUN 2021
Accepted 26 JUL 2021

Author Contributions:

Conceptualization: Raphaël Savelli, João Serôdio, Philippe Cugier, Vona Méléder, Pierre Polsenaere, Christine Dupuy, Vincent Le Fouest
Data curation: Raphaël Savelli
Formal analysis: Raphaël Savelli, Vincent Le Fouest
Funding acquisition: Christine Dupuy, Vincent Le Fouest
Investigation: Raphaël Savelli, João Serôdio, Philippe Cugier, Vona Méléder, Pierre Polsenaere, Christine Dupuy, Vincent Le Fouest
Methodology: Raphaël Savelli, João Serôdio, Philippe Cugier, Vona Méléder, Pierre Polsenaere, Vincent Le Fouest

Abstract Microphytobenthos (MPB) are a key primary producer of intertidal mudflats. MPB face strong variability in incident irradiance during low tides. Despite photoprotection and photoacclimation, such variations can translate into the photoinhibition of MPB cells. This study explores the effect of photoinhibition on MPB primary production (PP) over a large and productive temperate mudflat (Brouage mudflat, NW France). We used a regional and high-resolution tri-dimensional hydrodynamic model coupled to an MPB model with or without photoinhibition. Photoinhibition leads to a 20% (-0.79×10^3 t C) decrease of the simulated MPB PP over the entire mudflat. As the upper shore is exposed to light more frequently and longer than the lower shore, the decrease of MPB PP is higher on the upper shore (−29%) than on the lower shore (−5%). With the highest photosynthetically active radiation cumulated over the mudflat, the decrease of MPB PP due to photoinhibition is the highest during spring and spring tides (−22% and −23%, respectively). The model suggests MPB photoinhibition is sensitive to the photoacclimation status of MPB cells through the light saturation parameter. This first modeling attempt to account for MPB photoinhibition is highly constrained by our current theoretical knowledge and limitations on the MPB growth physiology, but it suggests that this process can have a substantial impact on the MPB PP. As such, assessing the MPB photosynthetic response to the highly variable environmental conditions that prevail in large and productive intertidal mudflats is a real challenge for quantifying MPB PP from a synoptic to inter-annual time scale.

Plain Language Summary Benthic micro-algae or microphytobenthos (MPB) inhabiting the surficial sediment sustain the high biological production of intertidal mudflats. MPB achieve photosynthesis by aggregating into a dense biofilm at the mud surface during daytime low tides. As MPB can be exposed to short-term variations and high light levels, they change their short-term physiology and position within the sediment to protect themselves. However, such strategies can be outbalanced by a too long stressful light exposure. In this study, we explore with a numerical model the impact of photoinhibition on MPB primary production (PP) over a large and very productive mudflat (NW France). The model suggests that photoinhibition can strongly impact MPB PP. With photoinhibition, the yearly PP decreases by 20% over the whole mudflat. The model suggests MPB PP is sensitive to the photoacclimation status of MPB cells, that is, their light use efficiency at a given light level. This first modeling attempt to account for MPB photoinhibition is highly constrained by our current theoretical knowledge and limitations on the MPB growth physiology, but it suggests that this process can have a substantial impact on the MPB PP.

1. Introduction

Benthic microalgae, or microphytobenthos (MPB), play a key role in the land-ocean continuum. MPB primary production (PP) sustains the high biological productivity of estuarine and shallow coastal areas, including intertidal mudflats (Hope et al., 2019; Pinckney, 2018). MPB PP largely supports benthic and pelagic secondary production in shallow water systems of the land-ocean continuum (Daehnick et al., 1992;

Project Administration: Raphaël Savelli, Pierre Polsenaere, Christine Dupuy, Vincent Le Fouest
Resources: Raphaël Savelli, Philippe Cugier, Pierre Polsenaere, Christine Dupuy, Vincent Le Fouest
Software: Raphaël Savelli, Philippe Cugier, Pierre Polsenaere, Vincent Le Fouest
Supervision: Raphaël Savelli, Philippe Cugier, Pierre Polsenaere, Christine Dupuy, Vincent Le Fouest
Validation: Raphaël Savelli
Visualization: Raphaël Savelli
Writing – original draft: Raphaël Savelli
Writing – review & editing: Raphaël Savelli, João Serôdio, Philippe Cugier, Vona Méléder, Pierre Polsenaere, Christine Dupuy, Vincent Le Fouest

Krumme et al., 2008; Miller et al., 1996; Moncreiff et al., 1992; Perissinotto et al., 2003; Smaal & Zurburg, 1997). MPB also stabilize the sediment upper layer by excreting extracellular polymeric substances that bind silt and clay particles and decrease the probability of sediment erosion (Paterson, 1989).

Incident light reaching the sediment surface varies within a wide range of intensity and on a short-term basis (Kühl et al., 1994). MPB cells can be exposed to high light levels at the sediment surface (higher than 2,000 μmol m^{-2} s^{-1}; Laviale et al., 2015). In response, MPB use physiological photoprotective mechanisms and photoprotective behaviors through phototaxis (Kromkamp et al., 1998; Laviale et al., 2015; Perkins et al., 2001). The balance between physiological and behavioral photoprotection varies with MPB growth forms (Barnett et al., 2015; Cartaxana et al., 2011; Jesus et al., 2009; Serôdio et al., 2012). In sandy sediments, incident light penetrates up to 3,000 μm (Cartaxana et al., 2011) and MPB are mostly composed of epipsammic diatoms that live in close association with sediment grains (Underwood, 2001) when free motile epipelic diatoms dominate MPB assemblages in muddy sediments (Underwood, 2001) for which light is strongly attenuated (photic layer of 600 μm; Cartaxana et al., 2011). Whereas, epipsammic diatoms exhibit high physiological photoprotection and low behavioral adaptations as their motility is restricted to the sphere of the sediment grains (Barnett et al., 2015; Cartaxana et al., 2011; Jesus et al., 2009; van Leeuwe et al., 2008), epipelic growth forms migrate vertically within the sediment to meet optimal light conditions. To cope with excess light, diatoms dissipate the excess of energy from light mostly through the Non-Photochemical Quenching of chlorophyll fluorescence (NPQ), which corresponds to de-epoxidation of xanthophyll pigments (diadinoxanthin to diatoxanthin) in the xanthophyll cycle (Lavaud & Goss, 2014). Diatoxanthin contributes to reduce the excitation energy reaching the PSII reaction centers. In epipsammic growth forms, the NPQ physiological photoprotection is often higher that in epipelic growth forms, compensated by vertical migrations (Raven, 2011; Serôdio et al., 2001, 2012).

MPB photoinhibition occurs when the excitation of PSII reaction centers induced by high light levels outbalances photoprotective mechanisms. Reactive oxygen species accumulate intracellularly and may cause the inactivation of PSII D1 protein involved in the protection of cellular structures. Thus, the decline of D1 protein and active PSII reaction centers decreases the photosynthetic efficiency and PP (Nishiyama et al., 2006). Photoinhibition of MPB photosynthesis was successfully measured in laboratory experiments (Frankenbach et al., 2018; Méléder et al., 2020; Serôdio et al., 2012). However, owing to the physiological and behavioral adaptations, it has rarely been observed in the field. Serôdio et al. (2008) reported *in situ* photoinhibition of an MPB assemblage due to incomplete recovery of the photosynthetic apparatus damaged from a previous light stress. In addition to light levels, the duration of exposure is of key importance in inducing photoinhibition of MPB photosynthesis as the longer the exposure to saturating light the higher the photo-damages (Blanchard et al., 2004; Henley, 1993; Pniewski & Piasecka-Jędrzejak, 2020; Serôdio et al., 2012).

Investigating the impact of MPB photoinhibition in light of photoprotective mechanisms on MPB PP is of high interest to budget the contribution of intertidal MPB to the C cycle in the land-ocean continuum. The goal of this study is to explore the potential impact of photoinhibition on MPB PP at the entire mudflat scale to the light of our best theoretical knowledge. For this purpose, we use a regional coupled physical-biological tri-dimensional (3D) model at high spatial resolution applied to the productive Brouage mudflat (NW France). In this study, we first describe the coupled physical-biological 3D model. Second, we describe the light environment over the studied mudflat and we assess the potential impact of photoinhibition on MPB PP. Finally, we discuss the spatial and temporal variability of MPB photoinhibition in the perspective of quantifying MPB PP from a synoptic (minute, hour, and day) to longer time scale (season, year, and decade) over large productive mudflats.

2. Material and Methods

2.1. Study Site

The study area is a shallow semi-enclosed sea on the French Atlantic coast called the Charentais Sounds Sea (Figure 1). The system is macrotidal and semi-diurnal with a tidal amplitude that ranges up to ~ 6 m during spring tides. The study site is the 42 km^2 intertidal Brouage mudflat located in the South-Eastern part of the study area (Figure 1). It is made up of fine cohesive sediments (median grain size 17 μm and 85%

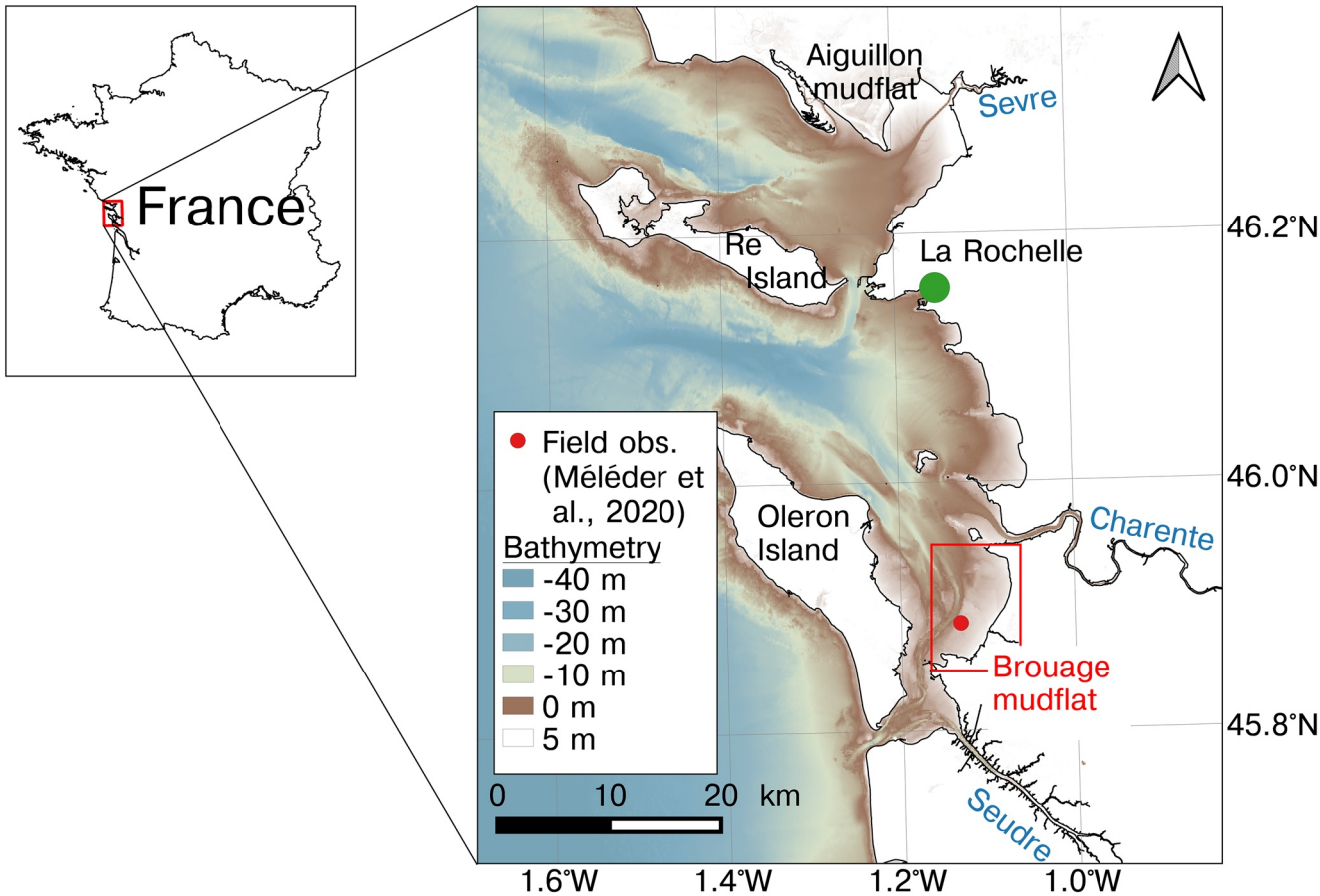

Figure 1. Bathymetry of the numerical domain of the model of the Charentais Sounds Sea (source: Service Hydrographique et Océanographique de la Marine). The study area is represented by the red box. The red point indicates the location of *in situ* observations from Méléder et al. (2020).

of grains with a diameter <63 μm; Bocher et al., 2007) and characterized by a gentle slope (~1/1,000; Le Hir et al., 2000) dominated by free motile epipelic diatoms.

2.2. Observations

In situ PP was measured by Méléder et al. (2020) on the lower shore of the Brouage mudflat (45°53′11.20″N, l°7′53.8″W; Figure 1) during spring and daytime low tides on May 5–6 and July 2–3, 2015. Méléder et al. (2020) derived nine PP estimates from C dioxide fluxes measured with benthic chambers at the air-sediment interface. The sampling protocol is fully described in Méléder et al. (2020).

2.3. The Coupled Physical-Biological 3D Model

2.3.1. The MARS-3D Modeling System

We used the MARS-3D (3D hydrodynamical Model for Applications at Regional Scale) circulation model to simulate the physical environment over the numerical domain shown in Figure 1. It includes the current velocity and direction, seawater temperature and salinity, tides, photosynthetically active radiation (PAR), and the mud surface temperature (MST). The model is a finite-difference model that solves the Navier-Stokes primitive equations under assumptions of Boussinesq approximation, hydrostatic equilibrium, and incompressibility (Blumberg & Mellor, 1987; Lazure & Dumas, 2008). A full description of the model is given in Lazure and Dumas (2008). The model was discretized into 100 m by 100 m horizontal grid cells and 20 σ vertical levels (terrain-following vertical discretization). Hourly atmospheric forcings (10 m wind speed, air temperature, atmospheric pressure at sea level, nebulosity fraction, relative humidity, and

solar fluxes) were provided by the Météo France AROME model (https://donneespubliques.meteofrance.fr/). Along the open boundaries of the numerical domain, the model was constrained by the amplitude and phase of 115 harmonic tidal constituents from the cstFRANCE tidal model developed by the French marine service for hydrography and oceanography (SHOM; Simon & Gonella, 2007). Boundary and initial conditions of seawater temperature, salinity, current velocity, and sea surface height were provided by the MANGAE 2500 Ifremer model (Lazure et al., 2009).

2.3.2. The Mud Surface Temperature Model

A mud temperature model fully detailed in Savelli et al. (2018) was coupled with MARS-3D. Thermodynamic equations detailed in Savelli et al. (2018) simulated heat fluxes within a 1 cm deep sediment layer. No horizontal fluxes were considered. During low tides, the simulated MST resulted from the heat energy balance that accounted for heat coming from the Sun and the atmosphere, leaving the sediment surface, from conduction between mud and air, and from mud evaporation. During high tides, the simulated MST was set to the temperature of the overlying seawater simulated by MARS-3D. The differential equation of heat energy balance between air and the sediment was solved by the MARS-3D numerical scheme. The comparison of the MST and PAR simulated by MARS-3D with space and time coincident *in situ* measurements (Méléder et al., 2020; Savelli et al., 2020) suggests that the MARS-3D modeling system can represent with confidence the physical environment at the study site.

2.3.3. The MPB Model

A MPB model was also coupled with MARS-3D. The conceptual MPB model and related differential equations are fully detailed in Savelli et al. (2018). The MPB model simulated the MPB biomass in the surface biofilm (S, mg Chl a m^{-2}) and in the sediment first centimeter (F, mg Chl a m^{-2}), and the gastropod *Peringia ulvae* biomass (Z, mg C m^{-2}) at the sediment surface. It accounted for vertical MPB migrations driven by diurnal and tidal cycles through exchanges of MPB biomass between S and F (Guarini et al., 2000). The MPB cells migrated upward within the sediment to form a productive biofilm during daytime low tides at the sediment surface. The MPB mass-specific photosynthetic rate P^b (mg C (mg Chl a)$^{-1}$ h^{-1}) was constrained by MST (°C) and PAR (W m^{-2}) according to the relationships of Blanchard et al. (1996) and Platt and Jassby (1976), respectively. In the model of Platt and Jassby (1976), the production-irradiance (P-E) relationship follows a sigmoid mathematical function in which photosynthesis saturates at the light saturation parameter (E_k), assumed to be constant over the year (100 W m^{-2}; Guarini et al., 2006; Savelli et al., 2018). The photosynthesis duration was determined by the mean time spent by MPB cells at the sediment surface (γ) and was set to 1.5 h according to Blanchard et al. (2004). At nightfall or at the flood beginning, the MPB cells migrated downward from S to F. The *P. ulvae* grazing on the MPB biofilm was constrained by the simulated MST and MPB biomass in the biofilm.

2.3.4. Photoinhibition of MPB

In the MPB model, during the first 1.5 h of daytime exposure, photoinhibition did not affect the photosynthetic capacity P^b_{max}. Beyond 1.5 h of daytime exposure, photoinhibition impacted MPB photosynthesis through a decrease of P^b_{max} only if PAR exceeded the light saturation parameter E_k according to the model of Blanchard et al. (2004):

$$\frac{dP^b_{max}}{dt} = \phi\left(P^b_M - P^b_{max}\right), \tag{1}$$

$$\frac{dP^b_M}{dt} = -P^b_M \frac{(\delta+1)}{\tau_s}\left(\frac{t}{\tau_s}\right)^{\delta}, \tag{2}$$

where τ_s is a time threshold (196 min) that drives the decrease of P^b_{max}, and P^b_M (mg C (mg Chl a)$^{-1}$ h^{-1}) is the maximum value of P^b_{max} when $t = \gamma$. ϕ (0.028 min^{-1}) is the inverse of the time for P^b_{max} to diverge from P^b_M. δ is a dimensionless parameter set at 2.69 that describes the photoinhibition intensity. The effect of MST on P^b_{max} superimposed on the effect of light (Figure 2c).

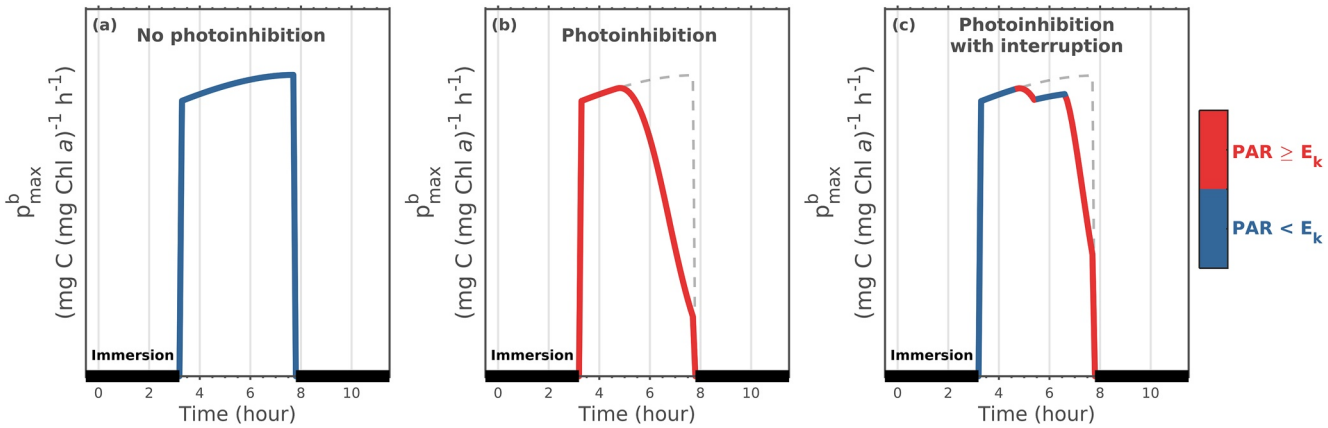

Figure 2. Conceptual representation of photoinhibition as a function of PAR intensity and duration of exposure in the model.

2.3.5. Model Set-Up

The initial conditions of the biological scalars F, S, and Z were set to 100 mg Chl a m^{-2}, 0 mg Chl a m^{-2} and 1,000 mg C m^{-2}, respectively. The MARS-3D modeling system was spun-up from September 12, 2014 00:00:00 UTC to January 1, 2015 00:00:00 UTC in order to converge toward balanced and realistic values of biomass on January 1 (Savelli et al., 2018, 2020). It was run from January 1, 2015 00:00:00 UTC to January 1, 2016 00:00:00 UTC. Two runs were performed, with (*Photo* run) and without (*NoPhoto* run) MPB photoinhibition.

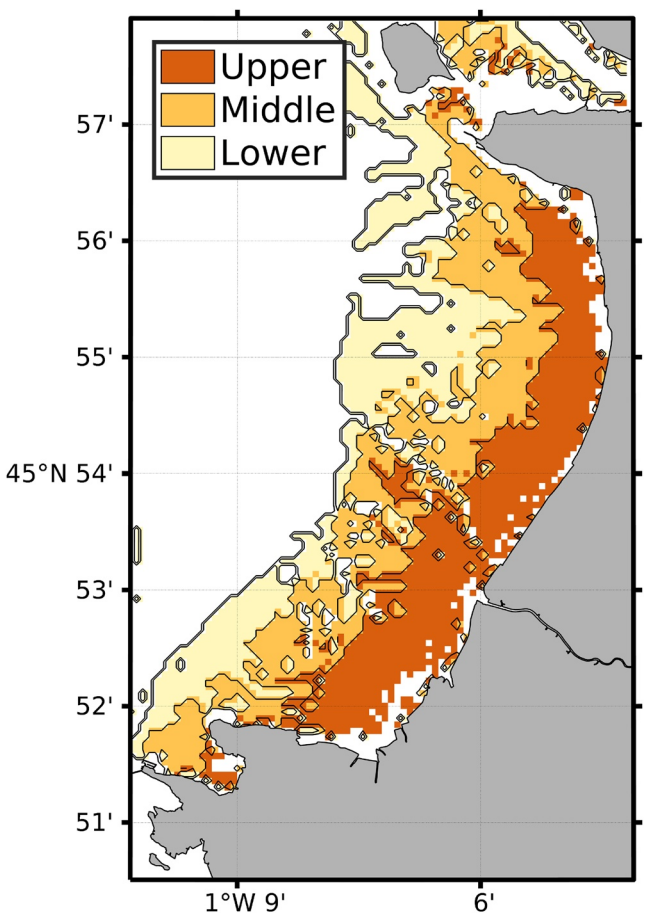

Figure 3. Tidal ranges computed according to the simulated tidal level.

2.3.5.1. Spatial and Temporal Analyses

The simulated mudflat emersion duration and periods, PAR intensity, and MPB PP were seasonally integrated during daytime emersions in winter (January–March), spring (April–June), summer (July–September), and fall (October–December). The simulated data were, when needed, averaged and integrated both in time and space over the whole Brouage mudflat or over three tidal ranges. Effectively productive mudflat pixels (annual MPB PP > 0; 35.8 km^2) were indeed divided in three equal areas (11.93 km^2) according to the mean duration of emersion simulated in 2015 (Figure 3). Such a partitioning distinguished the upper shore that emerged more than 5.15 h per day from the middle shore (2.9–5.15 h per day) and the lower shore (< 2.9 h per day). Spring tides were identified when the simulated daily maximal water height at a given model grid cell exceeded the 91.5th percentile of simulated water height over the year. The spatio-temporal variability of the total amount of PAR (PAR integral) reaching each part of the mudflat was investigated along with the number and the duration of emersion periods per day during each season.

2.3.5.2. Sensitivity Analyses

We tested the sensitivity of the simulated MPB photoinhibition to E_k and γ. E_k and γ were indeed identified as sensitive constants for simulated MPB PP (Savelli et al., 2018, 2019). We performed 8 runs with photoinhibition in which E_k and γ were varied while the other parameters were kept fixed at the value set in the reference *Photo* run. E_k varied within the observed range (2.5, 50, 150, 200 W m^{-2}; Savelli et al., 2018, and references within) and γ took values of 0.5, 1, 2 and 2.5 h. The model was run for the spring season, when the effect of photoinhibition on MPB was found

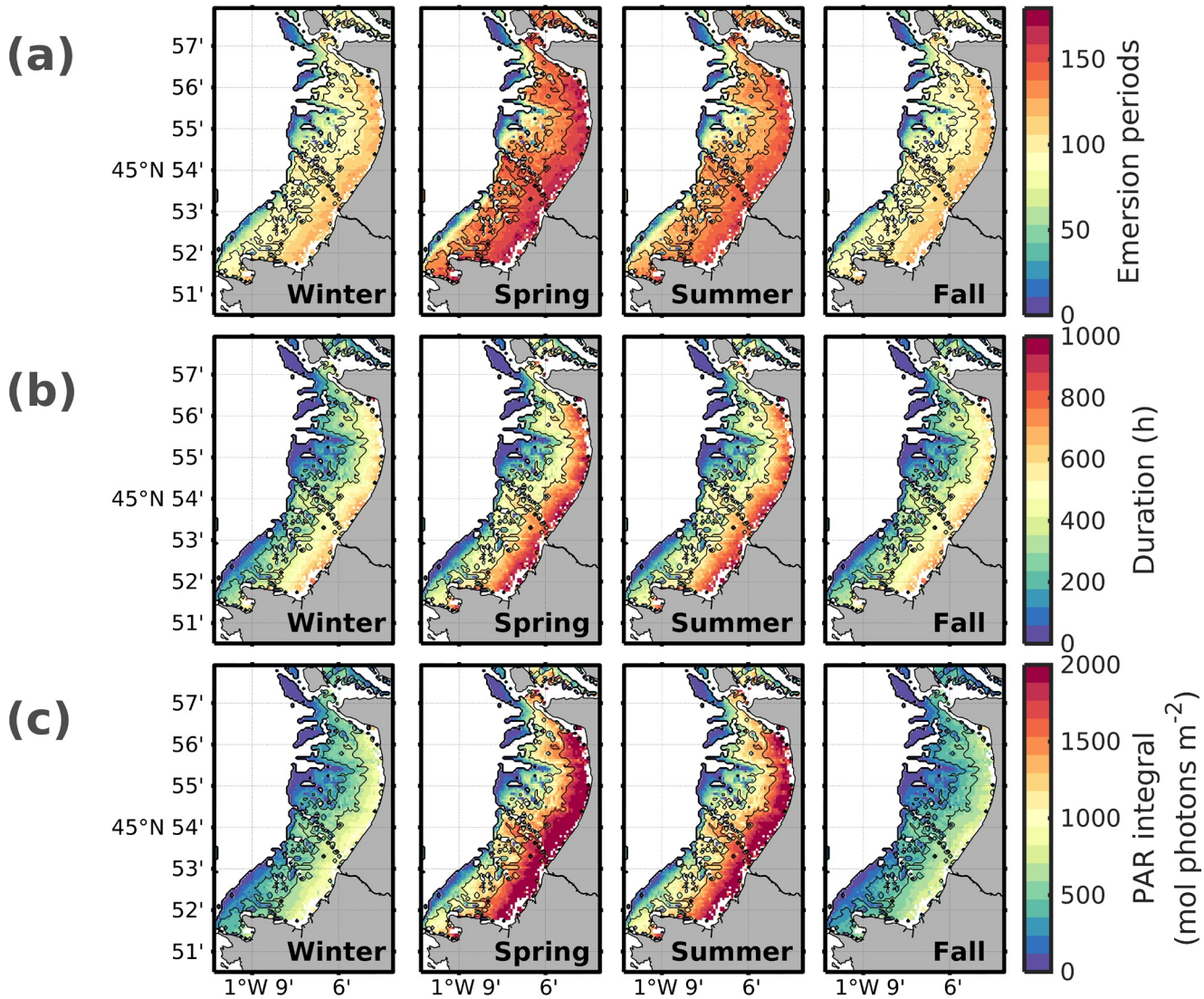

Figure 4. Distribution of the seasonally integrated simulated (a) Daytime emersion periods, (b) Daytime emersion duration (h) and, (c) Surface PAR (mol photons m^{-2}). The black contour lines delimitate the three tidal ranges.

to be the highest. The sensitivity of photoinhibition was assessed by comparing the simulated MPB PP from the 8 respective runs with that of the reference *Photo* run.

3. Results

3.1. Light Environment on the Mudflat

In the model, the cumulated number of daytime emersion periods decreased seaward (Figure 4a). Annually, the lower shore emerged 242 ± 143 times per year in average and rarely exceeded 1 daytime emersion period per day (0.7 ± 0.6 period per day) while the upper shore showed 516 ± 40 emersion periods per year in average i.e., 1.4 ± 0.6 daytime emersion periods per day. In spring and summer, the number of daily daytime emersions increased, especially on the middle and upper shores (Figure 4a).

The simulated daytime emersion duration also decreased seaward (Figure 4b). With 2,465 ± 440 h of daytime emersion per year in average, the upper shore emerged 6.8 ± 2.6 h per day in average that was two- to five-fold longer than on the middle and lower shores, respectively (1,468 ± 244 h and 465 ± 338 h i.e., 4 ±

Table 1
Mean Simulated (± Standard Deviation) MPB Biomass in the Sediment First cm (mg Chl a m^{-2}) With (Photo Run) and Without (NoPhoto Run) MPB Photoinhibition

Run	Season	Upper	Middle	Lower	All
NoPhoto	Winter	143.07 ± 89.6	117.5 ± 52.8	32.3 ± 48.2	43.2 ± 72.1
	Spring	60 ± 32.6	75 ± 20.8	31.5 ± 35.6	24.6 ± 35.7
	Summer	47.8 ± 28.1	58.2 ± 16.7	16.1 ± 21.5	18 ± 27.8
	Fall	70.7 ± 39.3	75.4 ± 17.9	20.3 ± 28.2	24.5 ± 37.3
	Annual	80.1 ± 64.7	81.2 ± 37.7	25 ± 35.3	27.6 ± 46
Photo	Winter	123.2 ± 72.1	109.3 ± 44	31 ± 45.2	38.9 ± 63.1
	Spring	54.9 ± 30.7	72.3 ± 20	31.1 ± 35.1	23.4 ± 34.3
	Summer	43.9 ± 25.5	55.2 ± 15.5	15.6 ± 20.8	16.9 ± 25.7
	Fall	65.7 ± 36.6	72.4 ± 16.3	19.6 ± 27.1	23.3 ± 35.4
	Annual	71.8 ± 54.3	77.1 ± 33.1	24.3 ± 34	25.6 ± 41.9

1.7 h and 1.3 ± 1.4 h per day, respectively). The upper and middle shores emerged longer in spring-summer compared to the other seasons (Figure 4b).

Because of emersion periods and duration, the yearly PAR simulated by the model reaching the sediment surface was not spatially uniform over the mudflat (Figure 4c). Through the seasons, the simulated PAR decreased seaward across the mudflat (Figure 4c). The yearly PAR on the upper shore was 5,107 ± 915 mol photons m^{-2} in average (i.e., an integral of 6.1×10^{10} mol photons), which was two- and five-fold higher than on the middle (3,111 ± 531 mol photons m^{-2} per year in average i.e., an integral of 3.7×10^{10} mol photons) and lower (1,080 ± 735 mol photons m^{-2} per year in average i.e., an integral of 1.3×10^{10} mol photons) shores, respectively. The simulated values were the highest in spring and summer and the lowest in fall, especially on the middle and upper shores (Figure 4c). In spring-summer, the PAR at the mud surface represented 70% of the yearly PAR.

3.2. Spatial and Temporal Variability of MPB PP

In both the Photo and NoPhoto runs, the simulated MPB biomass was higher on the upper and middle shores than on the lower shore (Table 1). In the *Photo* run, the highest decrease of MPB biomass occurred on the upper shore, where it decreased by 10% compared to the *NoPhoto* run (Table 1). MPB biomass on the lower shore reached similar levels in the *NoPhoto* and the *Photo* runs. The simulated seasonal cycle of MPB biomass was characterized by a winter maximum and a summer minimum on each tidal range (Table 1).

In both the *NoPhoto* and the *Photo* runs, the mean simulated annual PP was higher on the upper (177.2 ± 64.2 and 124.8 ± 46.2 g C m^{-2} yr^{-1} in the *NoPhoto* and the *Photo* runs, respectively) and middle shores (132.2 ± 29.4 and 113.5 ± 19.7 g C m^{-2} yr^{-1} in the *NoPhoto* and the *Photo* runs, respectively) than on the lower shore (32.9 ± 43.4 and 30.6 ± 38 g C m^{-2} yr^{-1} in the *NoPhoto* and the *Photo* runs, respectively) (Table. 2).

Table 2
Mean Simulated Annual Primary Production (± Standard Deviation) (g C m^{-2} yr^{-1})

Run	Upper	Middle	Lower	All
NoPhoto	177.2 ± 64.2	132.2 ± 29.4	32.9 ± 43.4	108.8 ± 79
Photo	124.8 ± 46.2	113.5 ± 19.7	30.6 ± 38	84.2 ± 57.7

3.3. Temporal Variability of MPB Photoinhibition

In the *Photo* run, PP simulated over the whole mudflat was lower than in the *NoPhoto* run for all seasons (Table 3). In the *Photo* run, the yearly PP over the whole mudflat decreased by 20% (-0.79×10^3 t C) compared to the *NoPhoto* run (Table 3). In both runs, the highest and the lowest PP were simulated in spring and fall, respectively (Table 3). MPB PP in winter and spring accounted for more than 60% of the yearly PP (Table 3). In

Table 3
Spatially and Seasonally Integrated Primary Production (10^3 t C) Simulated on Each Tidal Range

Run	Season	Upper	Middle	Lower	All
NoPhoto	Winter	0.58	0.43	0.12	1.13
	Spring	0.71	0.55	0.15	1.42
	Summer	0.36	0.3	0.06	0.73
	Fall	0.29	0.23	0.05	0.57
	Annual	1.95	1.52	0.38	3.85
Photo	Winter	0.41	0.37	0.11	0.89
	Spring	0.5	0.48	0.14	1.11
	Summer	0.26	0.26	0.06	0.58
	Fall	0.22	0.2	0.05	0.47
	Annual	1.39	1.31	0.36	3.06
Difference (10^3 t C)	Winter	−0.17	−0.06	−0.01	−0.24
	Spring	−0.21	−0.07	−0.01	−0.31
	Summer	−0.1	−0.04	< 0.01	−0.15
	Fall	−0.07	−0.03	< 0.01	−0.1
	Annual	−0.43	−0.21	−0.02	−0.79
Difference (%)	Winter	−29	−14	−8	−21
	Spring	−30	−13	−7	−22
	Summer	−27	−13	< −1	−20
	Fall	−24	−13	< −1	−17
	Annual	−29	−14	−5	−20

the Photo run, the lowest and the highest PP decrease over the whole mudflat occurred in fall (-0.1×10^3 t C i.e., −17%) and spring (-0.31×10^3 t C i.e., −21%), respectively (Table 3).

The decrease of the yearly MPB PP simulated over the whole mudflat was higher during spring tides (−23% i.e., -0.49×10^3 t C) than during neap tides (−18% i.e., -0.31×10^3 t C; Table 4). In the Photo run, the PP decrease simulated during neap tides was the highest in spring (−21% i.e., -0.14×10^3 t C) and the lowest in fall (−11% i.e., -0.03×10^3 t C; Table 4). During spring tides, the PP difference between the *NoPhoto* and *Photo* runs did not show high variations over the seasons (~ −22%; Table 4).

3.4. Spatial Variability of MPB Photoinhibition

In the *Photo* run, the simulated PP was lower than in the *NoPhoto* run at all ranges of the mudflat (Table 3). PP decreased seaward as also simulated in the *NoPhoto* run. The highest yearly PP was simulated on the upper shore in both the *Photo* (1.39×10^3 t C) and *NoPhoto* (1.95×10^3 t C) runs (Table 3). In both runs, the upper and middle shores accounted for ~ 90% of the yearly PP over the entire mudflat (Table 3). With photoinhibition, the decrease of yearly PP was higher on the upper shore (-0.43×10^3 t C, i.e., −29%) than on the middle shore (-0.21×10^3 t C, i.e., −14%; Table 3). By contrast, the decrease of yearly PP was low on the lower shore (-0.02×10^3 t C, i.e., −5%; Table 3).

Table 4
Primary Production Difference (%) Between the Photo and the NoPhoto Runs at Neap and Spring Tides

Tidal range	Winter	Spring	Summer	Fall	Annual
Neap tides	−17	−21	−18	−11	−18
Spring tides	−24	−22	−23	−21	−23

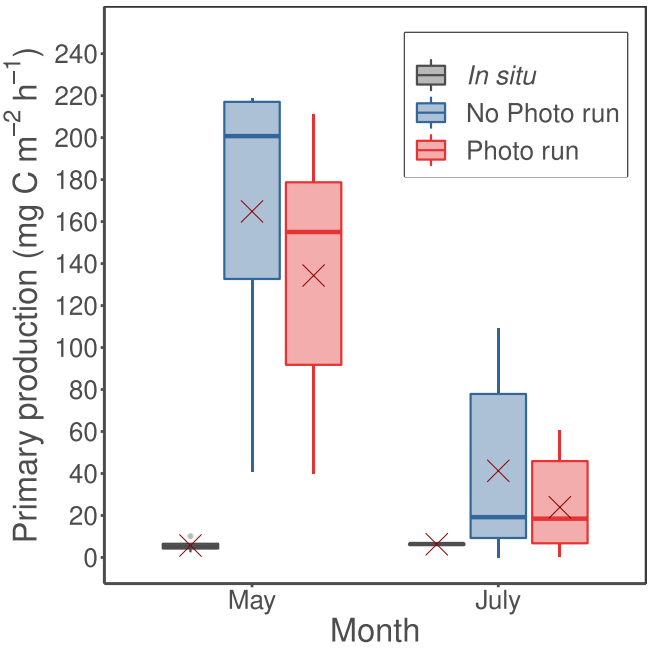

Figure 5. Measured and coincident simulated MPB PP (mg C m^{-2} h^{-1}) at the study site investigated by Méléder et al. (2020) in May and July 2015. Red crosses correspond to the mean value for the corresponding period. Modified from Savelli et al. (2020).

3.5. Sensitivity of the Model to the Photoinhibition Parameterization

Simulated PP rates in both runs were compared with measured PP at a specific location on the lower shore in May and July 2015 (Figure 1). Simulated PP rates in the *NoPhoto* and *Photo* runs in days matching *in situ* measurements (164.8 ± 66.7 and 134.3 ± 64.3 mg C m^{-2} h^{-1}, respectively) were on average 29–23-fold higher than the measured PP in May 2015 (5.69 ± 3.22 mg C m^{-2} h^{-1}; Figure 5). In July 2015, PP simulated in the *NoPhoto* run (41.3 ± 43.6 mg C m^{-2} h^{-1}) and in the *Photo* run (23.9 ± 23.4 mg C m^{-2} h^{-1}) were higher than *in situ* PP (6.3 ± 0.3 mg C m^{-2} h^{-1}; Figure 5). Simulated PP in the *Photo* run was in average 18% and 42% lower than in the *NoPhoto* run in May and July 2015, respectively (Figure 5). With photoinhibition, the model-observations gap was therefore reduced by 20% and 50% in average in May and July 2015, respectively (Figure 5).

The simulated MPB PP from the 8 respective sensitivity runs was compared with that of the reference *Photo* run during the spring season, when the effect of photoinhibition on MPB was found to be the highest. In the *Photo* run, the decrease of E_k induced an increase of MPB PP (Figure 6). With E_k set to 2.5 W m^{-2}, PP increased by ~38% and ~ 35% on the lower and the upper shore, respectively (Figure 6). With E_k set to 50 W m^{-2}, PP increased by 10% on the upper shore and by 15% on the middle and lower shores (Figure 6). Conversely, increasing E_k to 150 W m^{-2} induced a higher decrease of PP on the lower and middle shores (−12%) than on the upper shore (−9%; Figure 6). With E_k set to 200 W m^{-2}, PP decreased by 17% on the upper and middle shores and by 22% on the lower shore (Figure 6). With respect to the γ parameter, the lower γ the lower PP (Figure 6). With γ set to 0.5 h, PP decreased by 55% on the upper and middle shores and by 50% on the lower shore (Figure 6). With γ set to 1 h, PP decreased by 10% on the upper shore and by 2% on the middle and lower shores (Figure 6). With γ set to 2 h, PP increased by ~ 3% over the entire mudflat (Figure 6). With γ set to 2.5 h, PP increased by 8% on the upper and middle shores and by 4% on the lower shore (Figure 6).

4. Discussion

4.1. Spatio-Temporal Variability of MPB PP

Annual rates of MPB PP simulated in both the *NoPhoto* and *Photo* runs (108.8 ± 79 and 84.2 ± 57.7 g C m^{-2} yr^{-1}, respectively) compare to previous reported estimates simulated at the same study site in 2008, 2012, and 2015 (137.5 ± 11 g C m^{-2} yr^{-1} in average; Savelli et al., 2018, 2019, 2020). They are also within the range of PP estimates reported for other European mudflats (43.4–300 g C m^{-2} yr^{-1}; Frankenbach et al., 2020, and references therein). Integrated over the whole mudflat (42 km^2), simulated PP is 3.85 and 3.06×10^3 t C in the *NoPhoto* and *Photo* runs, respectively. Such values compare to ecosystem-level MPB PP estimates reported by Frankenbach et al. (2020, 5.6×10^3 t C over 34 km^2) and Haro et al. (2020, 0.45×10^3 t C over 13 km^2).

The seasonality of MPB PP depicted by the model is consistent with the one reported on the same mudflat by Méléder et al. (2020) using space remote sensing. In both the *NoPhoto* and *Photo* runs, the highest PP is simulated in winter and spring and represents ~ 65% of the yearly PP. The seasonal peak of PP is simulated in spring (1.42–1.11×10^3 t C), which agrees with the spring bloom of MPB PP reported at the study site (Cariou-Le Gall & Blanchard, 1995) and on others Northern European mudflats (Echappé et al., 2018; van der Wal et al., 2010).

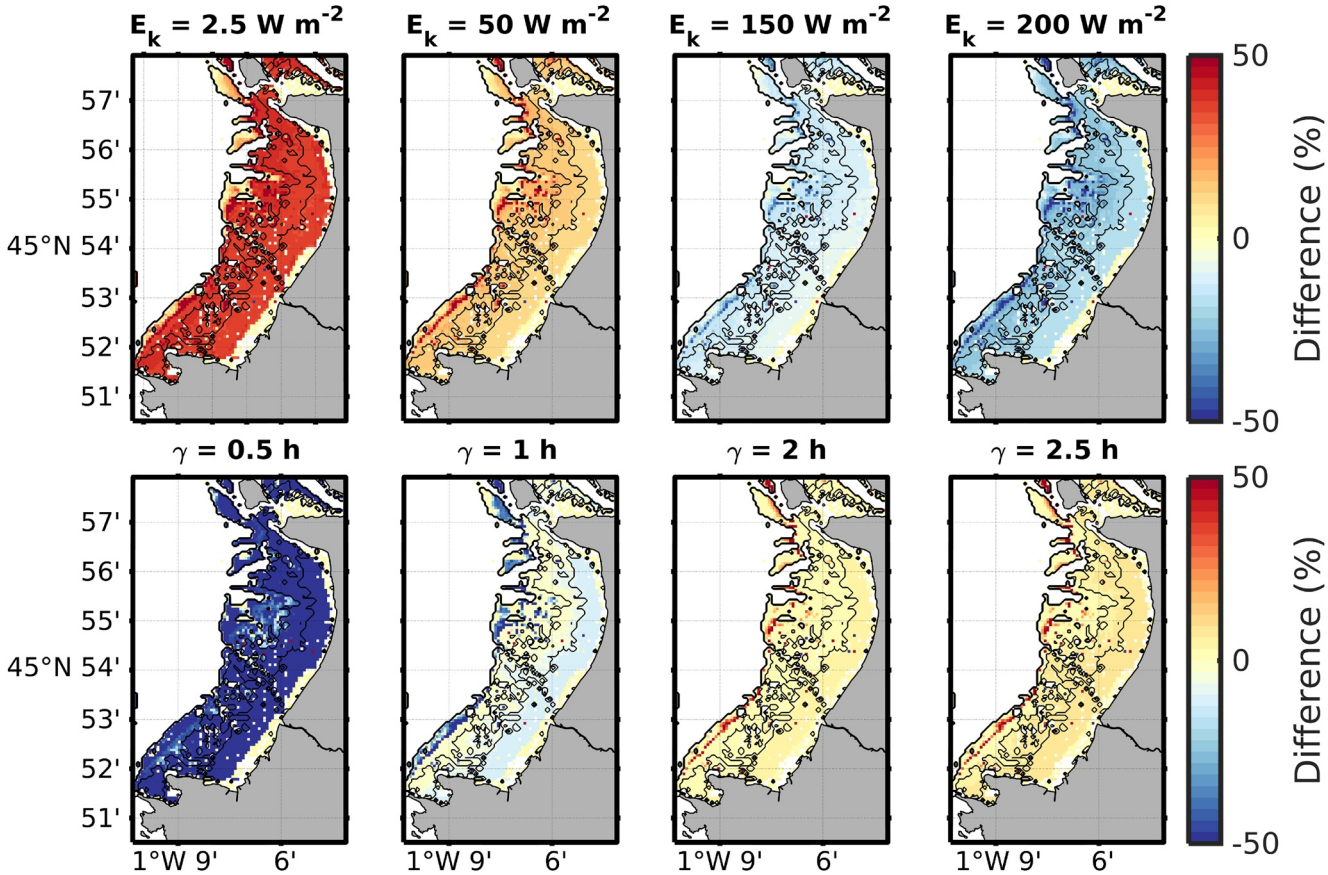

Figure 6. Microphytobenthos primary production (MPB PP) difference (%) between the *Photo* run and 8 runs set with photoinhibition characterized by different values of the light saturation parameter (E_k) and the mean time spent by MPB cells at the sediment surface (γ) during the spring season. The black contour lines indicate the three tidal ranges.

The simulated PP does not distribute evenly over the entire mudflat. PP is the highest on the upper and middle shores in both the *NoPhoto* and *Photo* runs due to more frequent and longer emersion periods. PP varies from 132 g C m^{-2} yr^{-1} on the middle shore to 177 g C m^{-2} yr^{-1} on the upper shore and from 113 to 125 g C m^{-2} yr^{-1} in the *NoPhoto* and the *Photo* runs, respectively. It contributes to 90% of the yearly PP simulated over the whole mudflat. A comparable spatial pattern was reported on a Brazilian sandflat, where PP rates measured with benthic chambers were the highest on the upper and middle shores (1.9–2.1 g C m^{-2} d^{-1} and 1.3–2.2 g C m^{-2} d^{-1}, respectively) compared to the lower shore (0.24–0.27 g C m^{-2} d^{-1}; Fonseca et al., 2008). CO_2 fluxes measured on a Tasmanian mudflat at the air-sediment interface were also reported to be higher on the upper (up to 15,000 μmol m^{-2} h^{-1}) than on the lower (up to 6,000 μmol m^{-2} h^{-1}) shore, suggesting a higher benthic PP on the upper zone (Cook et al., 2004).

4.2. Temporal Variability of Photoinhibition

In the model, the effect of photoinhibition on MPB is the highest in spring over the whole mudflat. It results from both increasing light levels and highest seasonal amplitude of spring tides at this season. The high amplitude of spring tides exposes the mudflat to a longer light exposure and coincides to noon when daily irradiance is the highest in the day. Such conditions promote MPB photoinhibition over the entire mudflat. By contrast, neap tides characterized by two low tides with a small tidal range occurring early and late in the day when the light levels and exposure duration are too low to trigger photoinhibition. Nevertheless, light levels are low enough to limit MPB growth without any contribution of photoinhibition (Savelli et al., 2018). On a South Korean mudflat, Kwon et al. (2014) also reported low *in situ* MPB PP rates at low light levels

during neap tides compared to spring tides. Our study suggests that spring tides conditions foster a higher MPB growth than during neap tides even if photoinhibitory light levels are more frequently reached.

The photoinhibition of MPB photosynthesis is often represented in P-E models by a decrease of photosynthesis at saturating irradiances such as in Eilers and Peeters (1988) and Platt (1980) models. However, these models may overestimate the effect of photoinhibition on photosynthesis, as they do not take into account for the time of exposure and recovery. We adapted the photoinhibition model previously set for constant light conditions (Blanchard et al., 2004) to account for the light history experienced by MPB during a full low tide and a prolonged exposure time. Photo-damages in the model are characterized by a decrease of the photosynthetic capacity (P^b_{max}) as a function of light exposure time. Such a model behavior is consistent with the decrease of the maximum quantum yield of PSII resulting from prolonged light stress observed *in situ* by Serôdio et al. (2008). In our study, the photo-damages simulated by the coupled model persist until the end of low tides. This result finds support in the work of Serôdio et al. (2008) that showed photo-damages experienced by MPB can alter its photosynthetic capacity until the early next emersion event. On the other hand, the observed recovery time of MPB photosynthetic efficiency can also occur within short time scales and reduce the time of photo-damages persistence (10–15 min; Ezequiel et al., 2015; Serôdio et al., 2012). In the absence of short-term recovery time, the model could have overestimated the effect of photoinhibition.

Regarding the relative consistency of the model of Blanchard et al. (2004) with literature, it appears to be the most appropriate model of MPB photoinhibition so far. However, as the model was estimated from epipelic diatoms suspensions, it differs from *in situ* conditions where photosynthetically active epipelic diatoms are arranged in biofilm at the sediment surface. The model captures therefore the theoretical light-response of MPB photosynthesis aside from light attenuation resulting from self-shading, migration behavior, and grain size (Forster & Kromkamp, 2004; Kühl et al., 1994; Serôdio, 2004). Laviale et al. (2015) and Serôdio et al. (2012) experimentally inhibited migration capacity of MPB biofilm cells and quantified a 20% decrease of the MPB quantum yield due to photoinhibition after a 3 h high light stress and a short recovery period (~ 10 min). Their results are consistent with the 20% decrease of the MPB photosynthetic capacity after a 3 h high light stress simulated by the model of Blanchard et al. (2004). Consequently, the agreement between the photoinhibition amplitude depicted by the model and literature suggests that the model can resolve with confidence the MPB photoinhibition in the absence of behavioral photoprotection. In addition, considering photoinhibition in the model contributes to reduce the gap between the seasonally parametrized MARS-3D model and synoptic measurements (Savelli et al., 2020). Aside from other drivers of MPB photosynthesis, such a convergence supports the hypothesis that MPB photoinhibition may occurred at the synoptic scale.

In the model, photoinhibition triggers when light levels exceed the light saturation parameter (E_k). E_k was reported to vary seasonally accordingly to the photoacclimation status of MPB cells (Blanchard & Cariou-Le Gall, 1994; Frankenbach et al., 2020; Pniewski et al., 2015). In the present study, according to Guarini et al. (2006) that did not detect any significant seasonal variations, E_k does not vary throughout the year. This contrast between studies can be attributed to differences in measurement conditions (slurry methods, suspended cells, *in situ*). Biofilm or sediment can indeed hinder the theoretical light-response of MPB photosynthesis due to light attenuation resulting from self-shading, migration behavior, and grain size (Forster & Kromkamp, 2004; Kühl et al., 1994; Serôdio, 2004). Regarding the high uncertainties around photosynthetic parameters estimation, it would be therefore too speculative to guess any changes of E_k. As a conservative approach, we preferred a model parametrization that was already validated with a constant E_k throughout the year (Savelli et al., 2018). Nonetheless, the sensitivity of the photoinhibition intensity to the photoacclimation status of MPB cells was simulated by making E_k vary over the spring season. The sensitivity analysis suggests that the lower the E_k value the higher the simulated MPB PP. By using a low E_k, the simulated increase of MPB PP due to more efficient photosynthesis at low irradiance compensates therefore the MPB PP decrease associated to a lower photo-inhibitory light threshold.

Alongside the light threshold for photoinhibition, the γ parameter sets the light exposure duration beyond which the decrease of the photosynthetic capacity initiates in the model. We set γ to 1.5 h according to the model of Blanchard et al. (2004), who measured a decrease of the photosynthetic capacity under saturating irradiance in controlled laboratory conditions. In situ, γ is likely to vary, as suggested by the observed time evolution of the maximum PSII quantum yield (Serôdio et al., 2008, Sébastien Lefebvre, personal communication, 2017). In the coupled model, the γ parameter also sets the photosynthesis duration of MPB cells.

A decrease of γ translates therefore into a decrease of the duration of photosynthesis and thus of MPB PP. This effect was already showed in Savelli et al. (2019). The increase of γ affects moderately the MPB PP as its effects is limited by the low tides duration.

4.3. Spatial Variability of Photoinhibition

In our analysis, we distinguish the upper and middle shores (high cumulated irradiance, high MPB production, and biomass) from the lower shore (low cumulated irradiance, low MPB production, and biomass). Light was previously identified as the key abiotic parameter driving the transversal variability in MPB PP on mudflats (Underwood & Kromkamp, 1999). In the coupled model, the upper and middle shores experience higher light exposure than the lower shore as they emerge longer and more frequently. Consequently, the upper and middle shores are more productive than the lower shore, where PP occurs over shorter periods of emersion. Upper and middle shore light conditions are more favorable for MPB in terms of photo-period compared to the lower shore (Underwood & Kromkamp, 1999). However, the longer and more frequent emersion periods simulated in the *Photo* run on the upper shore lead to the highest decrease of the yearly MPB PP (-0.43×10^3 t C). By contrast, the simulated MPB PP decreases by 0.02×10^3 t C on the lower shore. In the absence of photoprotective mechanisms, this result suggests that photoinhibition has a higher impact on MPB PP on the upper shore than on the lower shore.

In the model, we assume that MPB photoacclimation is spatially homogeneous over the entire mudflat. However, the sensitivity analysis suggests that simulated MPB take advantage of low light acclimation ($E_k <$ 100 W m^{-2}) on the lower shore, which translates into more efficient photosynthesis at low irradiance. Furthermore, the exposure duration on the lower shore is rarely long enough to induce photoinhibition since the emersion duration is shorter on the lower shore than on the upper shore. On the lower shore, simulated MPB only benefit from a low light acclimation ($E_k <$ 100 W m^{-2}). Conversely, a high light acclimatation status is more detrimental to MPB PP simulated on the lower shore, because photosynthesis is less efficient at similar light levels. In laboratory experiments, Ezequiel et al. (2015) showed that the photoacclimation status of MPB cells determines their light preferendum and phototaxis. Although there is no field evidence that low light-acclimated MPB cells avoid photoinhibitory light levels, such a spatial variability of photoacclimation in the model can temper or enhance the MPB capacity to cope with high light levels. Strong variations of the γ parameter have a greater effect on PP on the upper and middle shores, because MPB are longer exposed to photoinhibition at these tidal ranges.

Finally, combining photosynthetic parameters (i.e., light- and temperature-related parameters) along with a photoinhibition parameterization based on *in situ* MPB sampled on the upper shore of the Brouage mudflat provides a consistent parameterization of MPB photoacclimation and photoinhibition on the upper shore. Nevertheless, caution is required when applied to the middle and lower shores (Blanchard et al., 1997, 2004; Guarini et al., 2006). In addition, the lack of spatial variations in the MPB capacity to cope with stressful light levels may mis-estimate in the model the effect of photoinhibition.

4.4. The Effect of Mud Surface Temperature on Photoinhibition

In the model, the effect of photoinhibition on the MPB growth superimposes to that of thermoinhibition (Savelli et al., 2018). Such a combined effect finds support in field and laboratory observations. In spring and summer when high MST and desiccation driven by high and long exposure to solar irradiance prevail, MPB growth decreases owing to both photo- and thermoinhibition (Guarini et al., 1997; Underwood, 1994). Temperature higher than the optimal temperature for MPB growth lead to a decrease of the photosynthetic capacity (Salleh & McMinn, 2011) as a result of the de-activation of the C fixation enzymes as RUBISCO (MacIntyre et al., 1997). The photoprotective NPQ physiological mechanism also varies with temperature. At high temperature levels, some benthic diatoms species (*Amphora* cf. *coffeaeformis* and *Cocconeis* cf. *sublittoralis*) have a greater capacity to cope with high light levels through NPQ (Salleh & McMinn, 2011). The PSII photosynthetic apparatus and its structuring D1 protein can be altered by high light levels. The rate of D1 protein repair process is temperature dependent and it decreases with high temperature (Campbell et al., 2006). The exposure of MPB cells to high temperature could slow down the repair of the photodam-

aged D1 protein and thus the subsequent recovery of the pool of active PSII (Jensen & Knutsen, 1993; Long et al., 1994). Finally, high temperature (> 35 °C) reduce the MPB motility and thus their negative phototactic capacity to avoid photoinhibition under high irradiance levels (Cohn et al., 2003; Laviale et al., 2015). The detrimental effect of high MST on the cell motility is not accounted for in the model but might further be implicitly represented through a temperature-related representation of the migration capacity.

4.5. Impact of Photoinhibition on the Fate of MPB PP Over Large Productive Mudflats

With PP estimates ranging from (43.4–300 g C m^{-2} yr^{-1}; Frankenbach et al., 2020, and references therein), MPB PP contributes up to one third of the total C fixation in coastal environments (including mud and sandflats, salt marshes, seagrass beds and kelp forests) of the northwest European shelf (236–841 g C m^{-2} yr^{-1}; Legge et al., 2020). While most of MPB PP is transferred to benthic and pelagic secondary production and then respired back to the atmosphere, a part of C is retained in the system through molluscs shells calcification (Fodrie et al., 2017; Ware et al., 1992) or microbial recycling and reutilization by MPB in sediment surficial layers (Oakes & Eyre, 2014). MPB are therefore a pivotal pathway in the coastal C cycle and a reduction of MPB PP by 20% due to photoinhibition may significantly impact the quantity and nature of C available for other organisms. Consequently, the potential effect of MPB photoinhibition questions MPB C budgets estimated in the absence of photoinhibition and which can be exported to higher trophic levels (e.g., Saint-Béat et al., 2013) or to the coastal ocean (e.g., Saint-Béat et al., 2014; Savelli et al., 2019). Understanding drivers of MPB photosynthesis such as photoinhibition is therefore needed to improve the quantification of coastal C budgets and fluxes from a synoptic to interannual time scale.

5. Conclusions

This study is a first attempt to simulate the potential effect of photoinhibition on MPB PP and its spatial and temporal variability at the scale of a whole temperate mudflat under realistic field conditions using a 3D physical-biological coupled model. In situ and laboratory estimates of the impact of photoinhibition on MPB PP are very limited due to the very synoptic nature of MPB dynamics. Nevertheless, we paid very careful attention to highly constrain the model with the high quality data/observations we have available so far to extrapolate laboratory knowledge to large mudflats encompassing marked spatial physical gradients. Some mechanistic processes such as behavioral adaptations, vertical light attenuation within the biofilm, and the alteration of the MPB ability to cope with stressful light levels due to high mud temperature and desiccation are not taken into account in the model, because such observations are even more limited. Despite these limitations, this first large-scale modeling study can be seen as a baseline for future studies that could help improve the predictive ability of models to quantify C budgets over large and very productive mudflats and provides key highlights on MPB PP sensitivity to photoinhibition across the mudflat ranges and over a full seasonal cycle:

1. Characterized by longer and more frequent emersion periods, the upper and middle shores experience higher cumulated levels of incident irradiance than the lower shore over a year. At the mudflat scale, about 70% of the total annual irradiance reaches the mud surface in spring-summer
2. With or without photoinhibition, the simulated yearly MPB PP is higher on the upper and middle shores than on the lower shore
3. With photoinhibition, the yearly MPB PP decreases by 20% (-0.79×10^3 t C yr^{-1}) at the mudflat scale
4. Photoinhibition leads to a higher decrease of the simulated yearly MPB PP on the upper shore (−29%, i.e., -0.43×10^3 t C yr^{-1}) than on the lower shore (−5 %, i.e., -0.02×10^3 t C yr^{-1}).
5. Over the entire mudflat, the highest decrease of the simulated MPB PP is due to photoinhibition occurring in springtime (−22%, i.e., -0.31×10^3 t C) and during spring tides (−23%, i.e., -0.49×10^3 t C) as emersion periods coincide with the highest daily amplitude of solar irradiance at noon
6. Simulated MPB PP is sensitive to a decrease of the exposure time threshold for photoinhibition (γ), especially on the upper and middle shores since they emerge longer and more frequently than the lower shore. On the lower shore, simulated MPB PP is sensitive to change in the light saturation parameter (E_k) as it implies in the model a change in the simulated photoacclimation status of MPB cells.

MPB photoprotective mechanisms are generally assumed as the main strategy of defense to prevent photoinhibition. However, laboratory and field observations suggest that MPB photoinhibition overcomes the photoprotective mechanisms. Accounting for such fine physiological processes and their regulation by mud temperature might indeed lead to more realistic predictions of MPB PP by predictive models. This study suggests that resolving the scale of tidal ranges is necessary for a better understanding of how and to what extent photoinhibition can alter the MPB biomass and PP. Regional and high resolution 3D coupled physical-biological models are being developed for this purpose but they still require observations for their parameterization and validation. Intertidal mudflats are remote and difficult to monitor over relevant space and time scales but space remote sensing offers promising perspectives. For instance, surveys of MPB dynamics in the next coming years will benefit the retrieval of photosynthesis derived from solar-induced fluorescence gathered from the FLuorescence EXplorer (FLEX) sensor (2023) in tandem with SENTINEL 3 mission both carried by the European Space Agency. Such observations will help improve the models' ability to predict MPB PP and how climate change scenarios might impact future trajectories of the coastal C cycle.

Data Availability Statement

The model outputs presented in this study were archived in a ZENODO repository (http://doi.org/10.5281/zenodo.4290770).

Acknowledgments
The authors acknowledge Meteo France for providing meteorological data and the Service Hydrographique et Océanographique de la Marine (SHOM) for providing the digital elevation model. The authors acknowledge the Pôle de Calcul et de Données Marines (PCDM) for providing DATARMOR storage, data access and computational resources. This research was funded by the Center national d'études spatiales (CNES), the Center National de la Recherche Scientifique (CNRS, LEFE-EC2CO program), the Région Nouvelle-Aquitaine and the European Union (CPER/FEDER) and the Groupement d'Intérêt Public (GIP) Seine-Aval PHARESEE project and the DYCOFEL project, funded through the 2015 Fondation de France call "Quels littoraux pour demain?". RS was supported by a PhD fellowship from the French Ministry of Higher Education, Research, and Innovation.

References

Barnett, A., Méléder, V., Blommaert, L., Lepetit, B., Gaudin, P., Vyverman, W., et al. (2015). Growth form defines physiological photoprotective capacity in intertidal benthic diatoms. *The ISME Journal*, *9*(1), 32–45. https://doi.org/10.1038/ismej.2014.105

Blanchard, G. F., & Cariou-Le Gall, V. (1994). Photo synthetic characteristics of microphytobenthos in Marennes-Oléron Bay, France: Preliminary results. *Journal of Experimental Marine Biology and Ecology*, *182*(1), 1–14. https://doi.org/10.1016/0022-0981(94)90207-0

Blanchard, G. F., Guarini, J.-M., Dang, C., & Richard, P. (2004). Characterizing and quantifying photoinhibition in intertidal microphytobenthos. *Journal phycological*, *40*, 692–696. https://doi.org/10.1111/j.1529-8817.2004.03063.x

Blanchard, G. F., Guarini, J.-M., Gros, P., & Richard, P. (1997). Seasonal effect on the relationship between the photosynthetic capacity of intertidal microphytobenthos and temperature. *Journal of Phycology*, *33*(5), 723–728. https://doi.org/10.1111/j.0022-3646.1997.00723.x

Blanchard, G. F., Guarini, J., Richard, P., Ph, G., & Mornet, F. (1996). Quantifying the short-term temperature effect on light-saturated photosynthesis of intertidal microphytobenthos. *Marine Ecology Progress Series*, *134*, 309–313. https://doi.org/10.3354/meps134309

Blumberg, A. F., & Mellor, G. L. (1987). A description of a three-dimensional coastal ocean circulation model. *Three-Dimensional Coastal Ocean Models*, *4*, 1–16. https://doi.org/10.1029/co004p0001

Bocher, P., Piersma, T., Dekinga, A., Kraan, C., Yates, M. G., Guyot, T., et al. (2007). Site-and species-specific distribution patterns of molluscs at five intertidal soft-sediment areas in northwest Europe during a single winter. *Marine Biology*, *151*(2), 577–594. https://doi.org/10.1007/s00227-006-0500-4

Campbell, S. J., McKenzie, L. J., & Kerville, S. P. (2006). Photosynthetic responses of seven tropical seagrasses to elevated seawater temperature. *Journal of Experimental Marine Biology and Ecology*, *330*(2), 455–468. https://doi.org/10.1016/j.jembe.2005.09.017

Cariou-Le Gall, V., & Blanchard, G. F. (1995). Monthly HPLC measurements of pigment concentration from an intertidal muddy sediment of Marennes-Oléron Bay, France. *Marine Ecology Progress Series*, *121*(1–3), 171–179. https://doi.org/10.3354/meps121171

Cartaxana, P., Ruivo, M., Hubas, C., Davidson, I., Serôdio, J., & Jesus, B. (2011). Physiological versus behavioral photoprotection in intertidal epipelic and epipsammic benthic diatom communities. *Journal of Experimental Marine Biology and Ecology*, *405*(1–2), 120–127. https://doi.org/10.1016/j.jembe.2011.05.027

Cohn, S. A., Farrell, J. F., Munro, J. D., Ragland, R. L., Weitzell, R. E., Jr., & Wibisono, B. L. (2003). The effect of temperature and mixed species composition on diatom motility and adhesion. *Diatom Research*, *18*(2), 225–243. https://doi.org/10.1080/0269249x.2003.9705589

Cook, P. L., Butler, E. C., & Eyre, B. D. (2004). Carbon and nitrogen cycling on intertidal mudflats of a temperate Australian estuary. I. Benthic metabolism. *Marine Ecology Progress Series*, *280*, 25–38. https://doi.org/10.3354/meps280025

Daehnick, A. E., Sullivan, M. J., & Moncreiff, C. A. (1992). Primary production of the sand microflora in seagrass beds of Mississippi Sound. *Botanica Marina*, *35*(2), 131–140. https://doi.org/10.1515/botm.1992.35.2.131

Echappé, C., Gernez, P., Méléder, V., Jesus, B., Cognie, B., Decottignies, P., et al. (2018). Satellite remote sensing reveals a positive impact of living oyster reefs on microalgal biofilm development. *Biogeosciences*, *15*(3), 905–918. https://doi.org/10.5194/bg-15-905-2018

Eilers, P., & Peeters, J. (1988). A model for the relationship between light intensity and the rate of photosynthesis in phytoplankton. *Ecological Modelling*, *42*(3), 199–215. https://doi.org/10.1016/0304-3800(88)90057-9

Ezequiel, J., Laviale, M., Frankenbach, S., Cartaxana, P., & Serôdio, J. (2015). Photoacclimation state determines the photobehaviour of motile microalgae: The case of a benthic diatom. *Journal of Experimental Marine Biology and Ecology*, *468*, 11–20. https://doi.org/10.1016/j.jembe.2015.03.004

Fodrie, F. J., Rodriguez, A. B., Gittman, R. K., Grabowski, J. H., Lindquist, N. L., Peterson, C. H., et al. (2017). Oyster reefs as carbon sources and sinks. *Proceedings of the Royal Society B: Biological Sciences*, *284*(1859), 20170891. https://doi.org/10.1098/rspb.2017.0891

Fonseca, A., Brandini, N., da Costa Machado, E., & Brandini, F. P. (2008). Variação espacial e sazonal da produção primária microfitobêntica em uma planície entremarés subtropical, Baía de Paranaguá, Paraná-Brasil. *INSULA Revista de Botânica*, *37*, 19.

Forster, R. M., & Kromkamp, J. C. (2004). Modelling the effects of chlorophyll fluorescence from subsurface layers on photosynthetic efficiency measurements in microphytobenthic algae. *Marine Ecology Progress Series*, *284*, 9–22. https://doi.org/10.3354/meps284009

Frankenbach, S., Ezequiel, J., Plecha, S., Goessling, J. W., Vaz, L., Kühl, M., et al. (2020). Synoptic spatio-temporal variability of the photosynthetic productivity of microphytobenthos and phytoplankton in a tidal estuary. *Frontiers in Marine Science*, *7*, 170. https://doi.org/10.3389/fmars.2020.00170

Frankenbach, S., Schmidt, W., Frommlet, J. C., & Serôdio, J. (2018). Photoinactivation, repair and the motility-physiology trade-off in microphytobenthos. *Marine Ecology Progress Series*, *601*, 41–57. https://doi.org/10.3354/meps12670

Guarini, J.-M., Blanchard, G., & Richard, P. (2006). Modelling the dynamics of the microphytobenthic biomass and primary production in European intertidal mudflats. In *Functioning of microphytobenthos in estuaries* (pp. 187–226). Edita.

Guarini, J.-M., Blanchard, G. F., Gros, P., Gouleau, D., & Bacher, C. (2000). Dynamic model of the short-term variability of microphytobenthic biomass on temperate intertidal mudflats. *Marine Ecology Progress Series*, *195*, 291–303. https://doi.org/10.3354/meps195291

Guarini, J.-M., Blanchard, G. F., Gros, P., & Harrison, S. J. (1997). Modelling the mud surface temperature on intertidal flats to investigate the spatio-temporal dynamics of the benthic microalgal photosynthetic capacity. *Marine Ecology Progress Series*, *153*(1–3), 25–36. https://doi.org/10.3354/meps153025

Haro, S., Lara, M., Laiz, I., González, C. J., Bohórquez, J., Garcia-Robledo, E., et al. (2020). Microbenthic net metabolism along intertidal gradients (Cadiz Bay, SW Spain): Spatio-temporal patterns and environmental factors. *Frontiers in Marine Science*, *7*, 39. https://doi.org/10.3389/fmars.2020.00039

Henley, W. J. (1993). Measurement and interpretation of photosynthetic light-response curves in algae in the context of photoinhibition and diel changes. *Journal of Phycology*, *29*(6), 729–739. https://doi.org/10.1111/j.0022-3646.1993.00729.x

Hope, J. A., Paterson, D. M., & Thrush, S. F. (2019). The role of microphytobenthos in soft-sediment ecological networks and their contribution to the delivery of multiple ecosystem services. *Journal of Ecology*, *108*(3), 815–830. https://doi.org/10.1111/1365-2745.13322

Jensen, S., & Knutsen, G. (1993). Influence of light and temperature on photoinhibition of photosynthesis inspirulina platensis. *Journal of Applied Phycology*, *5*(5), 495–504. https://doi.org/10.1007/bf02182508

Jesus, B., Brotas, V., Ribeiro, L., Mendes, C., Cartaxana, P., & Paterson, D. (2009). Adaptations of microphytobenthos assemblages to sediment type and tidal position. *Continental Shelf Research*, *29*(13), 1624–1634. https://doi.org/10.1016/j.csr.2009.05.006

Kromkamp, J., Barranguet, C., & Peene, J. (1998). Determination of microphytobenthos PSII quantum efficiency and photosynthetic activity by means of variable chlorophyll fluorescence. *Marine Ecology Progress Series*, *162*, 45–55. https://doi.org/10.3354/meps162045

Krumme, U., Keuthen, H., Barletta, M., Saint-Paul, U., & Villwock, W. (2008). Resuspended intertidal microphytobenthos as major diet component of planktivorous Atlantic anchoveta Cetengraulis edentulus (Engraulidae) from equatorial mangrove creeks. *Ecotropica*, *14*, 121–128.

Kühl, M., Lassen, C., & Jørgensen, B. B. (1994). Light penetration and light intensity in sandy marine sediments measured with irradiance and scalar irradiance fiber-optic microprobes. *Marine Ecology Progress Series*, *105*, 139–148. https://doi.org/10.3354/meps105139

Kwon, B.-O., Koh, C.-H., Khim, J. S., Park, J., Kang, S.-G., & Hwang, J. H. (2014). The relationship between primary production of microphytobenthos and tidal cycle on the Hwaseong mudflat, west coast of Korea. *Journal of Coastal Research*, *30*(6), 1188–1196. https://doi.org/10.2112/jcoastres-d-11-00233.1

Lavaud, J., & Goss, R. (2014). The peculiar features of non-photochemical fluorescence quenching in diatoms and brown algae. In B. Demmig-Adams, G. Garab, W. AdamsIII, & Govindjee (Eds.), *Non-photochemical quenching and energy dissipation in plants, algae and cyanobacteria* (pp. 421–443). Springer Netherlands. https://doi.org/10.1007/978-94-017-9032-1_20

Laviale, M., Barnett, A., Ezequiel, J., Lepetit, B., Frankenbach, S., Méléder, V., et al. (2015). Response of intertidal benthic microalgal biofilms to a coupled light-temperature stress: Evidence for latitudinal adaptation along the Atlantic coast of Southern Europe. *Environmental Microbiology*, *17*(10), 3662–3677. https://doi.org/10.1111/1462-2920.12728

Lazure, P., & Dumas, F. (2008). An external-internal mode coupling for a 3D hydrodynamical model for applications at regional scale (MARS). *Advances in Water Resources*, *31*(2), 233–250. https://doi.org/10.1016/j.advwatres.2007.06.010

Lazure, P., Garnier, V., Dumas, F., Herry, C., & Chifflet, M. (2009). Development of a hydrodynamic model of the Bay of Biscay. Validation of hydrology. *Continental Shelf Research*, *29*(8), 985–997. https://doi.org/10.1016/j.csr.2008.12.017

Legge, O., Johnson, M., Hicks, N., Jickells, T., Diesing, M., Aldridge, J., et al. (2020). Carbon on the northwest European shelf: Contemporary budget and future influences. *Frontiers in Marine Science*, *7*, 143. https://doi.org/10.3389/fmars.2020.00143

Le Hir, P., Roberts, W., Cazaillet, O., Christie, M., Bassoullet, P., & Bacher, C. (2000). Characterization of intertidal flat hydrodynamics. *Continental Shelf Research*, *20*(12–13), 1433–1459. https://doi.org/10.1016/s0278-4343(00)00031-5

Long, S. P., Humphries, S., & Falkowski, P. G. (1994). Photoinhibition of photosynthesis in nature. *Annual Review of Plant Biology*, *45*(1), 633–662. https://doi.org/10.1146/annurev.pp.45.060194.003221

MacIntyre, H. L., Sharkey, T. D., & Geider, R. J. (1997). Activation and deactivation of ribulose-1, 5-bisphosphate carboxylase/oxygenase (Rubisco) in three marine microalgae. *Photosynthesis Research*, *51*(2), 93–106. https://doi.org/10.1023/a:1005755621305

Méléder, V., Savelli, R., Barnett, A., Polsenaere, P., Gernez, P., Cugier, P., et al. (2020). Mapping the intertidal microphytobenthos gross primary production part I: Coupling multispectral remote sensing and physical modeling. *Frontiers in Marine Science*, *7*, 520. https://doi.org/10.3389/fmars.2020.00520

Miller, D. C., Geider, R. J., & MacIntyre, H. L. (1996). Microphytobenthos: The ecological role of the "secret garden" of unvegetated, shallow-water marine habitats. II. Role in sediment stability and shallow-water food webs. *Estuaries*, *19*(2), 202–212. https://doi.org/10.2307/1352225

Moncreiff, C. A., Sullivan, M. J., & Daehnick, A. E. (1992). Primary production dynamics in seagrass beds of Mississippi Sound: The contributions of seagrass, epiphytic algae, sand microflora, and phytoplankton. *Marine Ecology-Progress Series*, *87*, 161–171. https://doi.org/10.3354/meps087161

Nishiyama, Y., Allakhverdiev, S. I., & Murata, N. (2006). A new paradigm for the action of reactive oxygen species in the photoinhibition of photosystem II. *Biochimica et Biophysica Acta (BBA)-Bioenergetics*, *1757*(7), 742–749. https://doi.org/10.1016/j.bbabio.2006.05.013

Oakes, J. M., & Eyre, B. D. (2014). Transformation and fate of microphytobenthos carbon in subtropical, intertidal sediments: Potential for long-term carbon retention revealed by ^{13}C-labeling. *Biogeosciences*, *11*(7), 1927–1940. https://doi.org/10.5194/bg-11-1927-2014

Paterson, D. M. (1989). Short-term changes in the erodibility of intertidal cohesive sediments related to the migratory behavior of epipelic diatoms. *Limnology and Oceanography*, *34*(1), 223–234. https://doi.org/10.4319/lo.1989.34.1.0223

Perissinotto, R., Nozais, C., Kibirige, I., & Anandraj, A. (2003). Planktonic food webs and benthic-pelagic coupling in three South African temporarily-open estuaries. *Acta Oecologica*, *24*, S307–S316, https://doi.org/10.1016/s1146-609x(03)00028-6

Perkins, R., Underwood, G., Brotas, V., Snow, G., Jesus, B., & Ribeiro, L. (2001). Responses of microphytobenthos to light: Primary production and carbohydrate allocation over an emersion period. *Marine Ecology Progress Series*, *223*, 101–112. https://doi.org/10.3354/meps223101

Pinckney, J. L. (2018). A mini-review of the contribution of benthic microalgae to the ecology of the continental shelf in the South Atlantic Bight. *Estuaries and Coasts*, *41*(7), 2070–2078. https://doi.org/10.1007/s12237-018-0401-z

Platt, T. (1980). Photoinhibition of photosynthesis in natural assemblages of marine phytoplankton. *Journal of Marine Research*, *38*, 687–701.

Platt, T., & Jassby, A. D. (1976). The relationship between photosynthesis and light for natural assemblages of coastal marine phytoplankton. *Journal of Phycology*, *12*(4), 421–430. https://doi.org/10.1111/j.0022-3646.1976.00421.x

Pniewski, F., Biskup, P., Bubak, I., Richard, P., Latała, A., & Blanchard, G. F. (2015). Photo-regulation in microphytobenthos from intertidal mudflats and non-tidal coastal shallows. *Estuarine, Coastal and Shelf Science*, *152*, 153–161. https://doi.org/10.1016/j.ecss.2014.11.022

Pniewski, F., & Piasecka-Jędrzejak, I. (2020). Photoacclimation to constant and changing light conditions in a benthic diatom. *Frontiers in Marine Science*, *7*, 381. https://doi.org/10.3389/fmars.2020.00381

Raven, J. A. (2011). The cost of photoinhibition. *Physiologia Plantarum*, *142*(1), 87–104. https://doi.org/10.1111/j.1399-3054.2011.01465.x

Saint-Béat, B., Dupuy, C., Agogué, H., Carpentier, A., Chalumeau, J., Como, S., et al. (2014). How does the resuspension of the biofilm alter the functioning of the benthos-pelagos coupled food web of a bare mudflat in Marennes-Oléron Bay (NE Atlantic)? *Journal of Sea Research*, *92*, 144–157. https://doi.org/10.1016/j.seares.2014.02.003

Saint-Béat, B., Dupuy, C., Bocher, P., Chalumeau, J., De Crignis, M., Fontaine, C., et al. (2013). Key features of intertidal food webs that support migratory shorebirds. *PLoS One*, *8*(10), e76739. https://doi.org/10.1371/journal.pone.0076739

Salleh, S., & McMinn, A. (2011). The effects of temperature on the photosynthetic parameters and recovery of two temperate benthic microalgae, Amphora CF. Coffeaeformis and Cocconeis CF. Sublittoralis (Bacillariophyceae). *Journal of Phycology*, *47*(6), 1413–1424. https://doi.org/10.1111/j.1529-8817.2011.01079.x

Savelli, R., Bertin, X., Orvain, F., Gernez, P., Dale, A., Coulombier, T., et al. (2019). Impact of chronic and massive resuspension mechanisms on the microphytobenthos dynamics in a temperate intertidal mudflat. *Journal of Geophysical Research: Biogeosciences*, *124*(12), 3752–3777. https://doi.org/10.1029/2019jg005369

Savelli, R., Dupuy, C., Barillé, L., Lerouxel, A., Guizien, K., Philippe, A., et al. (2018). On biotic and abiotic drivers of the microphytobenthos seasonal cycle in a temperate intertidal mudflat: A modelling study. *Biogeosciences*, *15*(23), 7243–7271. https://doi.org/10.5194/bg-15-7243-2018

Savelli, R., Méléder, V., Cugier, P., Polsenaere, P., Dupuy, C., Lavaud, J., et al. (2020). Mapping the intertidal microphytobenthos gross primary production, part II: Merging remote sensing and physical-biological coupled modeling. *Frontiers in Marine Science*, *7*(521). https://doi.org/10.3389/fmars.2020.00521

Serôdio, J. (2004). Analysis of variable chlorophyll fluorescence in microphytobenthos assemblages: Implications of the use of depth-integrated measurements. *Aquatic Microbial Ecology*, *36*(2), 137–152. https://doi.org/10.3354/ame036137

Serôdio, J., da Silva, J. M., & Catarino, F. (2001). Use of in vivo chlorophyll a fluorescence to quantify short-term variations in the productive biomass of intertidal microphytobenthos. *Marine Ecology Progress Series*, *218*, 45–61. https://doi.org/10.3354/meps218045

Serôdio, J., Ezequiel, J., Barnett, A., Mouget, J.-L., Méléder, V., Laviale, M., & Lavaud, J. (2012). Efficiency of photoprotection in microphytobenthos: Role of vertical migration and the xanthophyll cycle against photoinhibition. *Aquatic Microbial Ecology*, *67*, 161–175. https://doi.org/10.3354/ame01591

Serôdio, J., Vieira, S., & Cruz, S. (2008). Photosynthetic activity, photoprotection and photoinhibition in intertidal microphytobenthos as studied in situ using variable chlorophyll fluorescence. *Continental Shelf Research*, *28*(10), 1363–1375. https://doi.org/10.1016/j.csr.2008.03.019

Simon, B., & Gonella, J. (2007). *La marée océanique côtière*. Institut océanographique.

Smaal, A. C., & Zurburg, W. (1997). The uptake and release of suspended and dissolved material by oysters and mussels in Marennes-Oléron Bay. *Aquatic Living Resources*, *10*(1), 23–30. https://doi.org/10.1051/alr:1997003

Underwood, G. J. (1994). Seasonal and spatial variation in epipelic diatom assemblages in the Severn estuary. *Diatom Research*, *9*(2), 451–472. https://doi.org/10.1080/0269249x.1994.9705319

Underwood, G. J. (2001). Microphytobenthos. In J. H. Steele (Ed.), *Encyclopedia of ocean sciences* (pp. 1770–1777). Academic Press. https://doi.org/10.1006/rwos.2001.0213

Underwood, G. J., & Kromkamp, J. (1999). Primary production by phytoplankton and microphytobenthos in estuaries. In D. Nedwell, & D. Raffaelli (Eds.), *Estuaries* (Vol. 29, pp. 93–153). Academic Press. https://doi.org/10.1016/S0065-2504(08)60192-0

van der Wal, D., Wielemaker-van den Dool, A., & Herman, P. M. J. (2010). Spatial synchrony in intertidal benthic algal biomass in temperate coastal and estuarine ecosystems. *Ecosystems*, *13*(2), 338–351. https://doi.org/10.1007/s10021-010-9322-9

van Leeuwe, M. A., Brotas, V., Consalvey, M., Forster, R. M., Gillespie, D., Jesus, B., et al. (2008). Photoacclimation in microphytobenthos and the role of xanthophyll pigments. *European Journal of Phycology*, *43*(2), 123–132. https://doi.org/10.1080/09670260701726119

Ware, J. R., Smith, S. V., & Reaka-Kudla, M. L. (1992). Coral reefs: Sources or sinks of atmospheric co 2? *Coral Reefs*, *11*(3), 127–130. https://doi.org/10.1007/bf00255465